Journal of Alloys and Compounds 505 (2010) 592–597

Contents lists available at ScienceDirect

Journal of Alloys and Compounds

journal homepage: www.elsevier.com/locate/jallcom

Electrical, optical and photoelectrochemical properties of $BaSnO_{3-\delta}$ Applications to hydrogen evolution

S. Omeiri[a,b], B. Hadjarab[c], A. Bouguelia[b], M. Trari[b,*]

[a] Centre of Research in Physical and Chemical Analysis (C.R.A.P.C.), B.P. 248, RP 16004, Algiers, Algeria
[b] Laboratory of Storage and Valorization of Renewable Energies (USTHB), Faculty of Chemistry B.P. 32, Algiers, 16111, Algeria
[c] Laboratory of Solid Solutions (USTHB), Faculty of Physic B.P. 32, Algiers, 16111, Algeria

ARTICLE INFO

Article history:
Received 22 March 2009
Received in revised form 12 June 2010
Accepted 16 June 2010
Available online 25 June 2010

Keywords:
Electrode materials
Hetero-junction
Semiconductors
Grain boundaries
X-ray diffraction
Electrochemical reactions

ABSTRACT

Photoactive $BaSnO_{3-\delta}$ is synthesized at 1253 K under air free atmosphere. The oxygen deficiency leads to a concomitant reduction of Sn^{4+} ions and the transport properties suggest low lattice polaron conduction with activation energy of 0.16 eV. Above 445 K, a plateau region is observed in the thermal variation of the conductivity caused by oxidation process, i.e. oxygen capture. The absence of the electrochemical peak $Sn^{2+/4+}$ in the intensity-potential curve corroborates the delocalization of the stereo chemical pair Sn^{2+}: $5s^2$. From photoelectrochemical measurements, the band gap is 2.80 eV and the transition is directly allowed. Moreover, indirect transition occurs at 2.60 eV. The material exhibits a long-term chemical stability over the whole pH range. In KOH (0.5 M) solution, the semi-logarithmic plot gave a current density of 24 $\mu A\,cm^{-2}$ and a corrosion potential of $-0.447\,V_{SCE}$. The capacitance measurements and cyclic voltammetry indicate that the photoresponse of $BaSnO_{3-\delta}$ is characteristic of n-type conductivity with a flat band potential of $-0.87\,V_{SCE}$ and an electron density of $1.2 \times 10^{20}\,cm^{-3}$. The best quantum efficiency occurs at 400 nm and is attributed to a depletion width (15 nm) and a diffusion length (57 nm) compared to a large penetration depth (820 nm). The electrochemical impedance spectroscopy (EIS) reveals the presence of bulk contribution effect and the Nyquist response has been decomposed on R–C parallel circuit. As application, $BaSnO_{3-\delta}$ has been tested successfully for the hydrogen evolution under visible illumination when combined with the delafossite $CuFeO_2$ as sensitizer.

1. Introduction

The perovskites $ASnO_3$ in which A is commonly an alkaline earth are important sensor materials to detect various gases [1]. They have also been studied for possible applications of the light-to-electrical and/or chemical energy conversion [2], stable capacitors [3] and oxygen-permeable ceramic membranes [4]. $BaSnO_3$ is classified as a wide band gap semiconductor where the conduction band (CB), originating from σ anti bonding mixture of Sn: 5s-O^{2-}: 2p orbital, is separated from the broad valence band (VB) of anionic O^{2-}: 2p parentage by a gap exceeding 3 eV [5]. It is well established now that the transport properties of stannates can be significantly improved by either doping on both A- and Sn-sub lattices [6] with heterovalent ions or by oxygen deficiency [7]. The electrical conductivity changes considerably when heated under low oxygen partial pressure due to the redox equilibrium with the surrounding atmosphere. Electrons are dominant carriers in the perovskites and the oxide represents a valence compensated system where oxygen extraction from the crystal lattice occurs concomitantly with tin reduction [8]. Consequently, $ASnO_3$ are n-type semiconductors and increasing the unit cell (Ca → Ba) enhances the mobility of oxygen ions and the degree of reduction [9]. The electrical studies reported on $BaSnO_3$ so far have been limited to low temperatures, a transition occurs from hopping mechanism to a conduction governed by activation to the mobility edge [10]. The scattering is so small that the hopping occurs through equivalent sites with almost free carriers and activationness energy. The conduction occurs via adiabatic hops of low polaron and the increase of the conductivity reflects an enhancement in the mobility. In the solid solution $Ba_{1-x}La_xSnO_3$, the thermo electric power indicated that there is more charge carriers than that would follow nominal valence and this is due to oxygen vacancies [11]. However, the data at high temperatures are missing and to our knowledge, no studies have been dealt in this direction.

On the other hand, there have been many investigations aimed to improve the efficiency of wide band semiconductors in photoelectrochemical (PEC) devices. Most materials used for the water splitting are based mainly on titanium oxides. So, it seemed attractive to develop new active materials for PEC conversion. The oxides containing cations with nd^{10} configuration are among the most sta-

* Corresponding author. Tel.: +213 24 79 50; fax: +213 24 80 08.
E-mail address: labosver@gmail.com (M. Trari).

0925-8388/$ – see front matter © 2010 Elsevier B.V. All rights reserved.
doi:10.1016/j.jallcom.2010.06.081

ble materials in photoelectrochemistry. In order to have a large band bending at the interface semiconductor/electrolyte, i.e. an efficient charge separation of electron/hole (e^-/h^+) pairs, the junction electric field must be large [12]. This requirement supposes the electron affinity of the semiconductor to be as low as possible. In this optic, barium should decrease the electron affinity of $BaSnO_3$ and shifts the flat band potential cathodically. In addition, $BaSnO_3$ is no toxic and chemically long lived. These characteristics make it attractive for the solar energy conversion [13]. However, it suffers from the drawback of low quantum efficiencies resulting from the large gap absorbing the UV radiations which entails only 5% of the sunlight. The hetero-junctions allow the extension of the spectral photoresponse toward the visible region. Therefore, the main aim of the present work was the PEC characterization of deficient stannate $BaSnO_{3-\delta}$ to assess its photoactivity for the hydrogen production. The importance of hydrogen, as sustainable and clean energy, has been highlighted in the literature [14]. We have coupled the chemical stability of $BaSnO_{3-\delta}$ with the absorbance of the delafossite $CuFeO_2$ while attempting to provide photoelectrons with enough reducing ability to reduce water into hydrogen. $CuFeO_2$ is selected because of its low cost, small optical gap and chemical stability [15].

2. Experimental

$BaSnO_3$, prepared by solid state ceramic method [16], served as starting material for further heat treatment. Appropriate amounts of $BaCO_3$ (Prolabo, 99%) and prefired SnO_2 (Ventron, 99.9%) were homogenized in an agate mortar for 30 nm. The powder was cold pressed into pellets under uniaxial pressure of 5 kbar. The pellets were fired at 1323 K for 48 h in air after which they were reground and refired for a further 36 h to get a well-crystallized oxide. Reduction was achieved by sealing $BaSnO_3$ pellets in silica ampoule under low pressure (<1 mbar) and firing at 1253 K (10 K min^{-1}) overnight. The process was speeded up considerably when small amount of Fe was used as getter. $CuFeO_2$ powder has been synthesized by nitrate route as reported in our previous work [15]. The control of the phases purity and the refinement of the lattice constants were performed with X-ray diffraction (XRD) at a scan speed of 0.05° min^{-1} in the 2θ range (5–80°) using monochromatized Cu Kα radiation.

Care was taken to minimize contacts resistance. Silver past was deposited on both sides of the pellet and the electrical conductivity was measured by the standard two probe technique. The thermoelectric power (type of conductivity) was performed by the differential technique with a temperature gradient of ~10 K through the pellet. The thermo emf was measured with a digital micro voltmeter (Tacussel, Aris 20000, impedance 10^{12} Ω) while the temperature gradient was determined with a thermo couple (type K).

Copper wires were soldered on one face of the pellets with silver paint; the pellets were assembled in glass holders with insulating epoxy resin leaving a geometrical surface of 0.2 cm^2. A standard three-electrode cell has been used for PEC characterization: the working electrode, an auxiliary Pt cathode (1 cm^2) and a saturated calomel electrode (SCE) to which all the potentials were quoted. The intensity-potential $J(V)$ characteristics and the capacitance curves were plotted thanks to a Voltalab PGZ 301 potentiostat/galvanostat (Radiometer). The electrode was irradiated through a quartz window with a 500 W Xenon lamp whose output was passed trough a monochromator with 10 nm band pass. The light intensity was measured at each wavelength with a calibrated light-meter (Testo 545) placed at the same position of the electrode. The aqueous solution containing KOH (0.5 M) as supporting electrolyte was continually flushed with nitrogen. The capacitance was measured as a function of the potential with a rate of 10 mV step AC voltage signal at a frequency of 10 kHz and 10 mV peak to peak in magnitude. The complex impedance data were acquired using small amplitude wave signals through a frequency response analyzer in the frequency range (10^{-3}–10^5 s^{-1}) with ten points per decade.

The photocatalytic tests were carried out in a closed gas circulation equipped with a water cooled double walled reactor previously described in detail [17]. The reactor was placed in a fixed position to keep a constant light flux. The temperature was regulated by a thermo stated bath regulated at 323 ± 2 K. The light source consists of three tungsten lamps (200 W) providing 2.09×10^{19} photons s^{-1} and the powder was dispersed by magnetic stirring under constant agitation. Prior each run, the solution (Na_2SO_4, 10^{-2} M) was purged for 35 min with pure nitrogen. Hydrogen in the outgoing gas was identified by gas chromatography; the amount was evaluated volumetrically by means of a graduated burette and corrected from blank experiments. The solutions were prepared from reagents of analytical quality and twice distilled water.

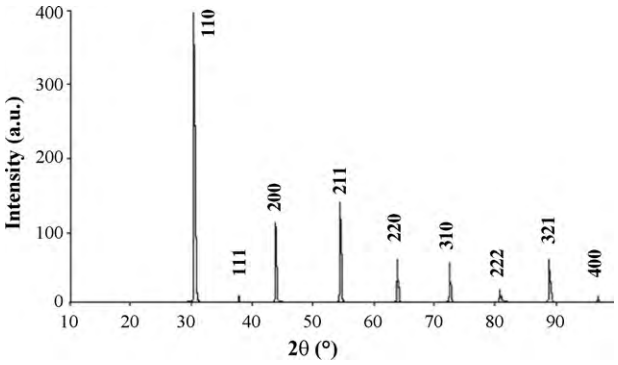

Fig. 1. XRD pattern of $BaSnO_{3-\delta}$ elaborated in silica tube.

3. Results and discussion

$BaSnO_{3-\delta}$ exhibits a blue color and the XRD pattern (Fig. 1) is indexed in a cubic unit cell as evidenced from the tolerance factor t (1.01: considering Shannon ionic radii). The lattice constant {a = 0.4117(2) nm; } is slightly larger than that of $BaSnO_3$ {0.4115(3) nm}; this implies an increase of the unit cell volume ($\Delta V = 0.0698\ nm^3$) induced by the oxygen under-stoichiometry. This is attributed to a small amount of Sn^{2+} ($r_{Sn^{2+}} = 0.110$ nm) in six-fold coordination [18], generated by a charge compensation mechanism, smaller than Sn^{4+} ($r_{Sn^{4+}} = 0.110$ nm). The materials with a Jahn–Teller ion bearing a lone pair like Sn^{2+} or Sb^{3+} crystallize in distorted structures with a low coordination environment and a limited composition range unless the lone pair ns^2 is delocalized in CB [19]. Under strong reducing atmosphere (H_2/Ar: 1/9), $BaSnO_3$ converts into SnO and β-Sn as proven by XRD and optical microscopy.

3.1. Transport properties

The high temperature defect chemistry of oxides and mechanism of transport properties have been well investigated in the past. In $BaSnO_3$, the ions Sn^{4+} occupy octahedral sites while Ba^{2+} are located in dodecahedrons and the perfect oxide is white and exhibits an insulating behavior [20,21]. The conductivity (σ) is extremely low and could not be measured, it can be assumed to be less than $10^{-8}\ \Omega^{-1}\ cm^{-1}$. However, σ is significantly increased by oxygen deficiency caused by equilibration under low oxygen partial pressure; the presence of iron (getter) lowers the partial oxygen pressure down to 10^{-6} atm. The system is electrically neutral and the formation of anionic vacancies occurs with Sn^{4+} reduction whose associated energy levels lie below the bottom of CB:

$$BaSnO_3 \rightarrow BaSn^{4+}_{1-\delta/2}Sn^{2+}_{\delta/2}O_{3-\delta} + 2\delta[e^-(CB)] + \delta/2O_2 \quad (1)$$

The conduction occurs by electron hopping through mixed $Sn^{4+/2+}$ions located in octahedra sharing common corners. The thermal variation $\sigma(T)$ indicates semi conducting behavior with a positive temperature coefficient, i.e. σ increases with increasing T and the data are well fitted by a polaron model: $\sigma = \sigma_o \exp -(\Delta E/kT)$ (Fig. 2, Inset), the pre-exponential constant σ_o is temperature independent. The activation energy ΔE ($0.16\ eV \ll 0.5E_g$), i.e. the separation between the Fermi level and CB, rules out any intrinsic conductivity. Consequently, the variation $\sigma(T)$ should result from a thermal activation of electrons, localized at the Fermi level. The released electrons are captured by Sn^{4+} ions to yield Sn^{2+} which act as donors shallows in conformity with n-type conductivity. This is explained in term of oxygen vacancies in accordance with the Kröger–Vink notation when the oxide is heated under oxygen free

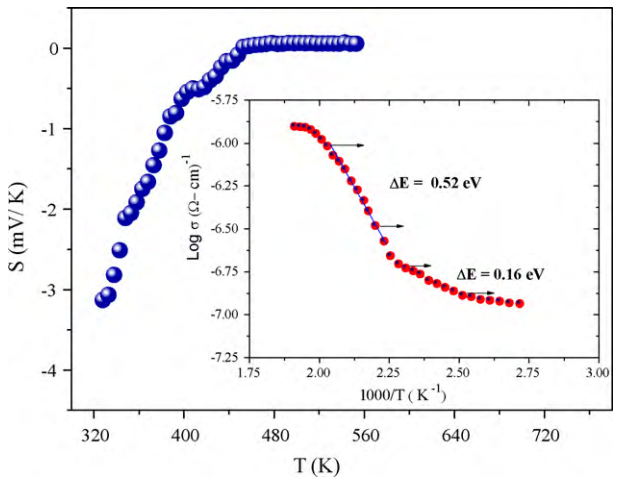

Fig. 2. The thermal variation of the thermo power of $BaSnO_{3-\delta}$. Inset: variation of $\log\sigma$ with 1000/*T*.

atmosphere:

$$O_O \leftrightarrow \tfrac{1}{2}O_2 + V_{\ddot{O}} + 2e^- \quad (2)$$

The vacancies promote the mass transport and recent studies revealed that the high temperature sintering of $BaSnO_3$ favors the densification, thus lowering the resistance of the grain boundaries.

Such process is enhanced because of the covalent character of the Sn–O bond, due to vaporation/condensation process [22].

In order to get insights into the nature of the conduction mechanism, we have determined the thermo power (*S*) on sintered pellets. *S* is measured with zero current and is less sensitive to the lattice imperfections and grain boundaries [21]. The conduction mechanism should be yet dominated by electron as *S* remains negative. Initially, $|S|$ rises with temperature up to 450 K ($\sim -40\,\mu V\,K^{-1}$) above which it remains nearly constant. The initial increase is attributed to ionization of donors. The little temperature dependence above 450 is consistent with non degenerate semiconductivity (Fig. 2) and is attributed to a thermal generation of electrons by impurity ionization (extrinsic process); *S* is expressed by [23]:

$$S = \left(\frac{-k}{e}\right)\ln\left(\frac{1-c}{c}\right) \quad (3)$$

where *c* is the ratio of the number of carriers to sites. For bosons lying in the impurity band, $c = 1/2$. An electron pairing is expected with post transition metals having lone pairs. The magnetic susceptibility was found to be positive and slightly temperature-dependent consistent with electron gas degeneracy [10]. The tin moments enable the carriers to form spin polarons. The existence of onsite bipolaron is ascribed to the tendency to Sn^{3+} ions to disproportionate into Sn^{2+} and Sn^{4+}. The process of oxygen extraction is reversible and the vacancies can be removed. The stoichiometry is entirely restored by heating the oxide in air up to 510 K, above which σ shows a plateau region and the color turns progressively to white with time heating.

3.2. Photoelectrochemistry

Preliminary tests showed that $BaSnO_3$ exhibits a chemical inertness over the whole pH range. A stable anode should have a small exchange current density J_{ex} and a low slope $\partial \log J/\partial V$, a J_{ex} value of 0.714 mA cm^{-2} was found in KOH (0.5 M) electrolyte (Fig. 3, Inset a). The electrochemistry is a sensitive technique to detect impurity phases as well as the presence of mixed valences in non degenerate semiconductors. The $J(V)$ characteristic (Fig. 3) shows that $BaSnO_{3-\delta}$ exhibits a good electrochemical stability with a dark current J_d less than 10 μA cm^{-2} and a rectifying junction at the electrolyte contact (chemical diode). Additional support of the delocalization of the inert pair Sn: $5s^2$ is brought by the missing of the peak corresponding to the electrochemical couple $Sn^{4+/2+}$ and which should theoretically appear at ~−0.1 V (depending on the substrate). A large current flows below ~−0.5 V, due to H_2 evolution.

As expected for n-type SC, the photocurrent (J_{ph}) is observed in the anodic region. The photocurrent onset potential V_{on}, taken as the potential above which J_{ph} could be observed can be assimilated to the potential V_{fb}. Upon scanning the potential toward positive

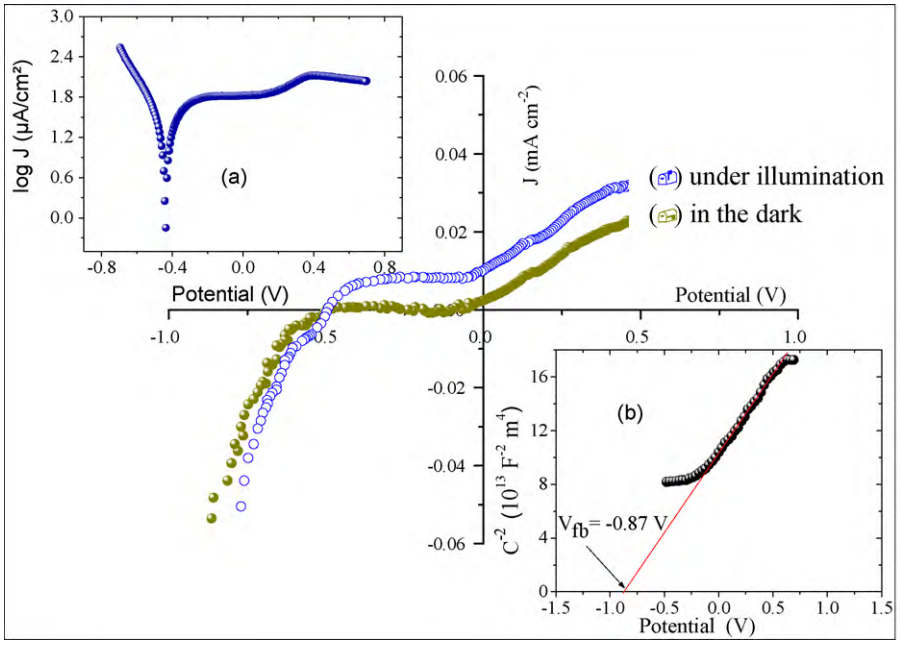

Fig. 3. The $J(V)$ characteristics of $BaSnO_{3-\delta}$ plotted both in the dark and under illumination, in KOH (0.5 M) electrolyte. Inset (a) Semi-logarithmic plot of the current density vs. potential. Inset (b) The corresponding Mott–Schottky plot.

values, J_{ph} appears at −0.5 V and increases gradually before reaching saturation at ~0.3 V. However, the accurate V_{fb} value has been obtained from the differential capacitance, measured at a frequency of 10 kHz:

$$C^{-2} = 2(\varepsilon\varepsilon_o eN_D)^{-1}\left(V - V_{fb} - \frac{kT}{e}\right) \quad (4)$$

where all the symbols have their usual significations. The potential V_{fb} (−0.87 V) and the density N_D (1.20×10^{20} cm^{-3}) were obtained respectively by extrapolating the curve to $C^{-2} = 0$ and from the slope of the linear part (Fig. 3, Inset b). The permittivity ε (=500) of $BaSnO_3$ was taken from Ref. [24]. The positive slope confirms the n-type character which is obviously the result of oxygen vacancies. The V_{fb} value should give rise to large band bending at the interface $BaSnO_3$/electrolyte with the existence of a depletion layer (W):

$$W = \left\{\frac{2\varepsilon\varepsilon_0(V - V_{fb})}{eN_D}\right\}^{0.5} \quad (5)$$

The width W, equal to 7 nm for a band bending ($V - V_{fb}$) of 0.5 V, extends over many crystallographic units. The optical characterization and hence the gap is a dominant property of any oxide while determining its application for PEC conversion. The quantum yield (η), measured with monochromatic light, was determined by dividing the electron flow in the external circuit (from the photocurrent J_{ph}) by the incident photon flux determined with a calibrated photodiode at each wavelength:

$$\eta = \frac{(J_{ph} - J_d)}{e\Phi} \quad (6)$$

Φ being the light intensity falling on the electrode and e the elementary charge. The electrode was biased at – 0.25 V, a value belonging to the plateau region in the $J_{ph}(V)$ curve. The $\eta(\lambda)$ characteristic clearly shows the existences of two wavelength ranges (Fig. 4a) which allow the determination of interband optical transitions [25]:

$$(\alpha h\nu)^n = A(h\nu - E_g) \quad (7)$$

The plot with $n = 2$ is linear whose intercept with $h\nu$ axis yields E_g-value of 2.80 eV (Fig. 4b), close to that determined previously [5]. Further transition ($n = 1/2$), indirectly allowed occurs at 2.60 eV (Fig. 4c). The electric current in SC is the sum of two components; the first one is attributed to carriers present in the depletion width W whereas the second one is due to carriers generated within the diffusion length L_D. When the determining step in PEC process is the rate of electrons flow, η is given by

$$\eta = 1 - \frac{[\exp(-\alpha W)]}{(1 + \alpha L_D)} \quad (8)$$

η is proportional to the optical absorption coefficient α if both the quantities αW and $\alpha L_D \ll 1$ [26]. Combining Eqs. (5) and (8), one obtains:

$$-\ln(1 - \eta) = \alpha\left(\frac{2\varepsilon\varepsilon_o}{eN_D}\right)^{1/2}(V - V_{fb})^{1/2} + \mathrm{Ln}(1 + \alpha L_D) \quad (9)$$

From the linear part of $-\ln(1 - \eta)$ against $(V - V_{fb})^{1/2}$ (Fig. 5), the parameters α (12195 cm^{-1}) and L_D (57 nm) have been determined at λ_{max} (400 nm).

The electrochemical impedance spectroscopy (EIS) is a powerful technique for the analysis of electrical behavior of the junction $BaSnO_3$/solution. It was measured at the open circuit potential (OCP, +0.324 V) in the frequency range (10^{-3}–10^5 Hz) and allows to distinguish between the various conduction mechanisms. The exchange of majority carriers through the interface is represented by the Nyquist plot (Fig. 6). The arc at high frequencies is attributed to the bulk contribution, i.e. faradic charge transfer and the intersection with the potential axis lead to the resistance of the charge

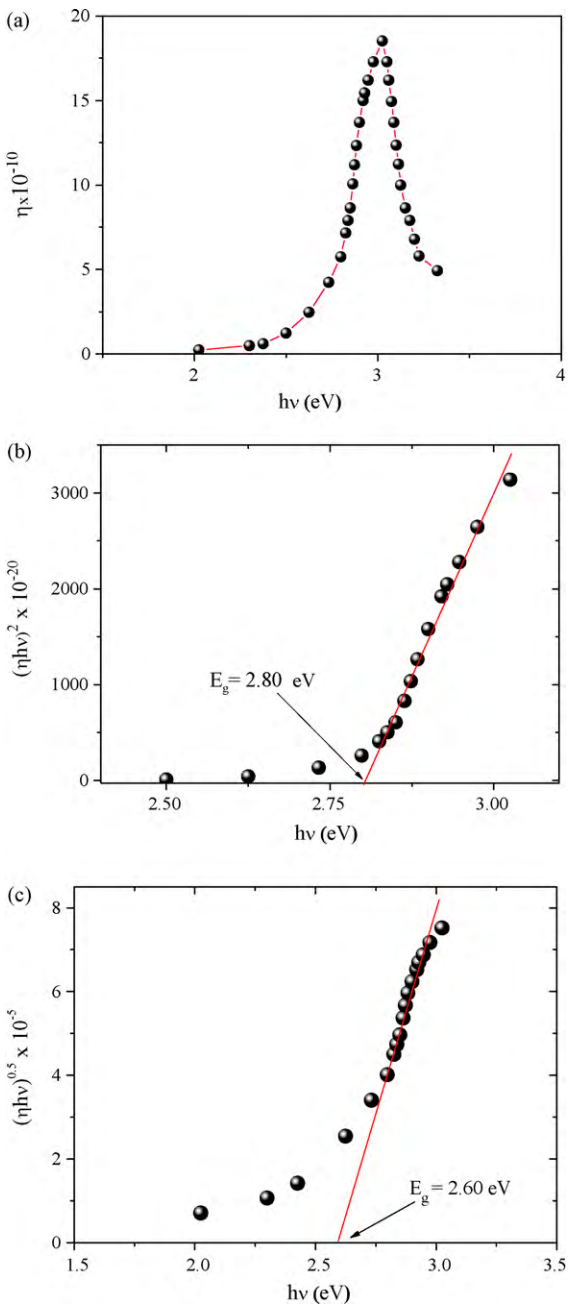

Fig. 4. (a) The quantum efficiency η of $BaSnO_{3-\delta}$ in KOH (0.5 M) solution. (b) Plotted as $(\eta h\nu)^2$ of the direct gap. (c) Plotted as $(\eta h\nu)^{1/2}$ of the indirect gap.

transfer R_{ct} (88.9 kΩ cm^2). The absence of arc at low frequencies indicates a small effect of grain boundaries in conformity with the high compactness of the pellet. Another hypothesis is that the relaxation times of the bulk and grain boundaries contributions are close to each other resulting in an arc overlapping. We also note a slight offset near the origin indicating a low series resistance attributed to the ionic electrolyte R_{el} (175 Ω cm^2). The experimental data were refined by the least square method thanks to the Randles model. The centre of the arc is localized below the real axis with an angle of 11°. The depletion, expressed by a constant phase element (CPE), is due to the inhomogeneity of the electrode. Such behavior can be attributed to various phenomena such as surface states, the porosity of the electrode, the distribution of current and potential field as well as slow adsorption [27]. The above results can be represented by a equivalent circuit (Fig. 6, Inset), composed of the resistance R_{ct}

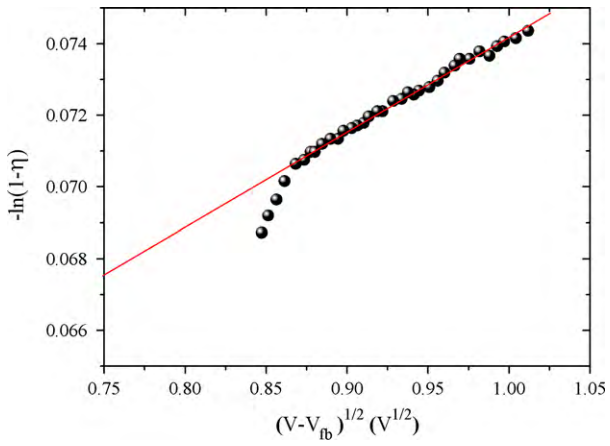

Fig. 5. Plot of $\ln(1-\eta)$ vs. $(V-V_{fb})^{1/2}$.

in parallel with CPE which in turn are connected in series with the electrolyte resistance R_{el}.

To our knowledge, only one paper is devoted to the hydrogen formation on stannates [28]. Unlike pellets, the crystallite cannot be polarized electrochemically. So, a further condition to eventuate in photoreductions is that OCP must be more positive than the potential V_{fb}. In addition, the crystallite is cathodically biased at OCP lower than the photodecomposition potential and the corrosion would be therefore prevented. The potential of $BaSnO_3$–CB ($V_{fb} - \Delta E = -4.1$ eV/−0.64 V), using 4.74 as the work function of SCE, indicates a conduction band made up Sn^{4+}: 5s orbital. In neutral solution (Na_2SO_4, 10^{-2} M), $BaSnO_3$–CB is more cathodic than the potential of the couple H_2O/H_2 (−0.5 V) and should give rise to a spontaneous hydrogen evolution. The latter was determined from the $J(V)$ characteristic under similar conditions. This hypothesis has been checked experimentally by illuminating a powder suspension with visible radiation (Fig. 7). However, in practice most of the sun spectrum is sub band gap and therefore not converted. Hence, $BaSnO_{3-\delta}$ exhibits a weak performance for H_2-production under one sun (air mass 1.5). An alternative to improve the photoactivity, i.e. to shift the spectral photoresponse of $BaSnO_{3-\delta}$ toward longer wavelengths and to improve the charges separation involves the hetero-junctions. The delafossite $CuFeO_2$ exhibits a dark blue color

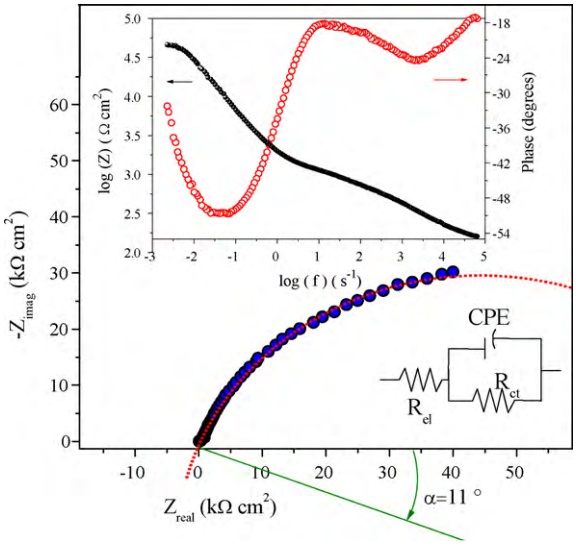

Fig. 6. Complex impedance spectroscopy of $BaSnO_{3-\delta}$ in KOH (0.5 M) solution with the equivalent circuit. Inset: Bode plots for $BaSnO_{3-\delta}$.

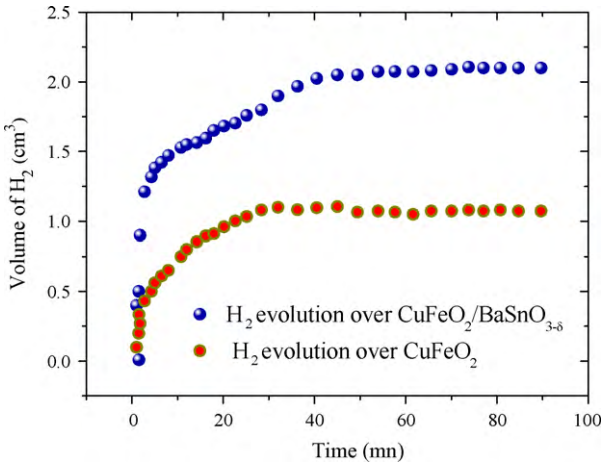

Fig. 7. Times course of the volume of H_2 over $CuFeO_2$ and the hetero-junction $CuFeO_2/BaSnO_{3-\delta}$.

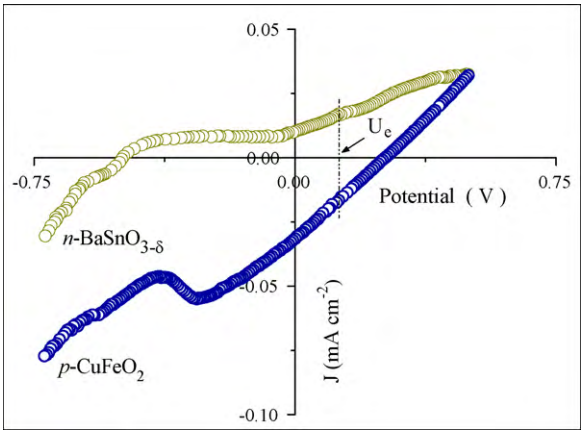

Fig. 8. Working characteristics of the hetero-junction n-$BaSnO_{3-\delta}$/p-$CuFeO_2$, derived from separate $J(V)$ curves under visible light.

with a gap of 1.32 eV [15] and is a good sensitizer since its conduction band (∼−1 V) is positioned at a potential more negative than $BaSnO_3$–CB. Preliminary experiments led us to select a pH 7 and the hetero-junction p-$CuFeO_2/n$-$BaSnO_{3-\delta}$ has been tested successfully for the hydrogen evolution. The cascade photochemical cell has the potential for achieving solar energy conversion [27]. The enhancement is attributed to the electron transfer from $CuFeO_2$–CB to $BaSnO_{3-\delta}$–CB resulting in the water reduction. One can derive the power characteristic from the two separate $J(V)$ curves of n-$BaSnO_{3-\delta}$ and p-$CuFeO_2$ (Fig. 8). The system operates ideally with negligible resistance and the equilibrium potential U_e (0.126 V) is obtained by connecting of the points where the anodic and cathodic current densities (17 μA cm^{-2}) balance to each other.

4. Conclusion

The electrical conductivity of $BaSnO_{3-\delta}$ was strongly enhanced by heating the stochiometric oxide under inert atmosphere. The electro neutrality is achieved by oxygen deficiency with concomitant reduction of Sn^{4+} ions and n-type conductivity. The conduction occurs by electron hopping through mixed valent $Sn^{4+/2+}$ ions accommodated in octahedral sites. The temperature dependence of the resistivity and thermo power reveals non degenerate conductivity at high temperatures. The insulating properties are totally restored by heating the deficient oxide in air. The lack of the peak is due to $Sn^{4+/2+}$ electrochemical couple lends further support to the

delocalization of the inert pair Sn^{2+}: $5s^2$. The flat band potential and the doping density were determined from the Mott–Schottky characteristic. The PEC measurements indicated an upper valence band primarily of oxygen character. The potential of the conduction band is positioned below the water reduction level and $BaSnO_{3-\delta}$ was found to be a potential candidate to generate hydrogen. This hypothesis has found an experimental support and $BaSnO_{3-\delta}$ has been tested successfully for the H_2 evolution under visible light. The activity of $BaSnO_{3-\delta}$ was significantly improved when combined with the delafossite $CuFeO_2$.

Acknowledgements

The authors would like to thank Mr D Bouteldja for his technical assistance. The financial support by the Faculty of Chemistry (Algiers) is acknowledged.

References

[1] H. Cheng, Z. Lu, Solid State Sci. 10 (2008) 1042.
[2] S. Upadhyay, O. Parkash, D. Kumar, J. Alloys Compd. 432 (2007) 258.
[3] A. Aydi, S. Chkoundali, H. Khemakhem, A. Simon, R. Von Der Mühll, J. Alloys Compd. 465 (2008) 222.
[4] W. Lu, S. Jiang, D. Zhou, S. Gong, Sens. Actuators 80 (2000) 35.
[5] B. Hadjarab, A. Bouguelia, A. Benchettara, M. Trari, J. Alloys Compd. 461 (2006) 360.
[6] M. Trari, J.P. Doumerc, P. Dordor, M. Pouchard, G. Behr, G. Krabbes, J. Phys. Chem. Solids 55 (1994) 1239.
[7] B. Hadjarab, A. Bouguelia, M. Trari, J. Phys. Chem. Solids 68 (2007) 1499.
[8] J. Cerdà, J. Arbiol, G. Dezanneau, R. Díaz, J.R. Morante, Sens. Actuators B 84 (2002) 21.
[9] O.I. Prokopalo, Ferroelectrics 14 (1976) 683.
[10] B. Hadjarab, A. Bouguelia, M. Trari, J. Phys. D: Appl. Phys. 40 (2007) 5833.
[11] B. Hadjarab, S. Bassaid, A. Bouguelia, M. Trari, Physica C 439 (2006) 67.
[12] P. Lemasson, A. Etcheberry, J. Gautron, Electrochim. Acta 27 (1982) 607.
[13] Alexander D.Q. Li, Lin Song Li, J. Phys. Chem. B 108 (2004) 12842.
[14] S. Ekambaram, J. Alloys Compd. 448 (2008) 238.
[15] S. Omeiri, Y. Gabès, A. Bouguelia, M. Trari, J. Electroanal. Chem. 614 (2008) 31.
[16] T. Badapanda, S.K. Rout, L.S. Cavalcante, J.C. Sczancoski, S. Panigrahi, T.P. Sinha, E. Longo, Mater. Chem. Phys. 121 (2010) 147.
[17] A. Derbal, S. Omeiri, A. Bouguelia, M. Trari, Int. J. Hydrogen Energy 33 (2008) 4274.
[18] R.D. Shannon, Acta Crystallogr. A 32 (1976) 751.
[19] I.A. Souza, M.F.C. Gurgel, L.P.S. Santos, M.S. Goes, S. Cava, M. Cilense, I.L.V. Rosa, C.O. Paiva-Santos, E. Longo, Chem. Phys. 322 (2006) 343.
[20] I.A. Souza, A.Z. Simoes, E. Longo, J.A. Varela, P.S. Pizani, Appl. Phys. Lett. 88 (2006) 211911.
[21] T. Badapanda, S.K. Rout, L.S. Cavalcante, J.C. Sczancoski, S. Panigrahi, E. Longo, M. Siu Li, J. Phys. D: Appl. Phys. 42 (2009) 175414.
[22] I.A. Souza, L.S. Cavalcante, J.C. Sczancoski, F. Moura, C.O. Paiva-Santos, J.A. Varela, A.Z. Simões, E. Longo, J. Alloys Compd. 477 (2009) 877.
[23] N.F. Mott, E.A. Davis, Electronic Processes in Non-Crystalline Materials, Clarendon, Oxford, 1979.
[24] J.I. Pankove, Optical Processes in Semiconductors, Prentice Hall, New Jersey, 1971.
[25] X.Y. Wei, X. Yao, Mater. Sci. Eng. B 137 (2007) 184.
[26] S.J. Xia, W.F. Zhou, Electrochem. Acta 40 (1995) 175.
[27] R. Brahimi, Y. Bessekhouad, A. Bouguelia, M. Trari, J. Photochem. Photobiol. A: Chem. 194 (2008) 173.
[28] W.F. Zhang, Junwang Tang, Jinhua Ye, Chem. Phys. Lett. 418 (2006) 174.